

**Chapter 23** 1  
**Ensemble Adaptive Data Assimilation** 2  
**Techniques Applied to Land-Falling** 3  
**North American Cyclones** 4

**Brian C. Ancell and Lynn A. McMurdie** 5

**23.1 Introduction** 6

Adaptive data assimilation is becoming an increasingly important aspect of numerical weather prediction. Traditional data assimilation involves combining a set of *routine* observations with a first-guess field provided by a numerical weather prediction model to produce an analysis of the atmospheric state. These analyses subsequently serve as the initial conditions for extended forecasts. There are three primary modern data assimilation methods that assimilate routine observations at operational centers around the world and within a number of research applications: (1) three-dimensional variational (3DVAR) systems, (2) four-dimensional variational (4DVAR) systems, and (3) ensemble Kalman filter (EnKF) systems. Each of these techniques are based on the assumption that the errors of both the first-guess, or background, variables and the observations are distributed normally, and aim to identify the most likely atmospheric state within the statistical framework of Bayes' Theorem (overview provided in Kalnay 2003).

Adaptive data assimilation allows the consideration of observational impact in some way beyond the aggregate effects of a set of routine observations. There are two primary types of adaptive data assimilation: (1) observation impact, and (2) observation targeting. Observation impact methods estimate the relative impact of each assimilated observation, or any subset of assimilated observations, on a chosen forecast metric. In turn, these techniques are able to identify which observations are important, and which are redundant, with regard to a number

AQ2

AQ1

---

B.C. Ancell (✉)  
 Department of Geosciences, Texas Tech University, Lubbock, TX 79409, USA  
 e-mail: Brian.Ancell@ttu.edu

L.A. McMurdie  
 Dept. of Atmospheric Sciences, University of Washington, Box 351640,  
 Seattle WA 98195-1640, USA

of different forecast aspects. The benefit of observation impact schemes is that they perform the assimilation of numerous observations only once to estimate the impact of each observation, removing the need to perform a large number of experiments (assimilating different observations each time) to achieve the same goal. Observation targeting methods estimate the impact from hypothetical observations that could be taken beyond an initial set of assimilated observations, revealing the locations where additional observations should be taken to produce the most benefit to a chosen forecast metric. In this way, targeting methods can be used to indicate the optimal placement of additional observational platforms. One attractive aspect of both observation impact and targeting approaches is that they easily allow the consideration of a specific forecast metric that diagnoses different sensible and high-impact weather events, such as localized wind speed or regional precipitation amount. Thus, these methods will likely have important applications in the future to answer a key question: what is the best way to observe the atmosphere to improve forecasts of specific severe weather phenomena?

This chapter reviews some of the leading observation impact and targeting methods today, gives a discussion of their evolution from older techniques, and applies one such targeting approach within an ensemble framework to a particular high-impact weather event: land-falling mid-latitude cyclones on the west coast of North America. Through this application, a variety of basic observation targeting characteristics of a specific data assimilation/forecasting system can be learned with regard to a specific, high-impact weather event, and include (1) the most important observation type to target, (2) whether targeting regions occur in the same location for different events or if they span a wide range of horizontal and vertical locations, and (3) if the relative impacts of targeted observations depend on the specific nature of the event (e.g. deepening or decaying cyclones) for which one is trying to improve the forecast. The application portion of this chapter addresses each of these three characteristics for Pacific land-falling North American cyclones.

## 23.2 The Evolution of Adaptive Data Assimilation Techniques

Early objective adaptive data assimilation techniques focused mostly on observation targeting, and addressed primarily the dynamical growth of forecast errors. Adjoint sensitivity (overview provided by Errico 1997) or singular vector methods (summarized in Kalnay 2003) were both employed to understand where analysis errors would grow rapidly, regardless of the data assimilation procedure used in creating the analyses. Atmospheric adjoint sensitivity was first derived in LeDimet and Talagrand (1986), and can be represented with the following equation:

$$\partial R / \partial \mathbf{x}_0 = \mathbf{M}_{t,0}^T * \partial R / \partial \mathbf{x}_t \quad (23.1)$$

where  $M_{t,t_0}^T$  is the transpose of the tangent-linear operator matrix obtained by linearizing the forcing terms of the full nonlinear forecast model equations, and  $\partial R/\partial \mathbf{x}_t$  is the differentiated response function  $R$  with respect to the atmospheric state at forecast time. The response function  $R$  can be any differentiable function of the forecast state variables, and is typically chosen to diagnose a specific aspect of the atmospheric state, such as low-level wind speed or localized precipitation amount. The term  $\partial R/\partial \mathbf{x}_o$  exists at every model grid point and represents the adjoint sensitivity of  $R$  with respect to the initial-time atmospheric state. For large sensitivity values, small perturbations to the initial-time atmospheric state will result in large perturbations to the forecast response function  $R$ . On the other hand, very large initial-time perturbations hardly influence  $R$  where sensitivity values are very small. In turn, adjoint sensitivity reveals regions where analysis errors would grow rapidly to cause large errors in the forecast response function  $R$ , revealing areas where it would be undesirable to have initial condition error.

Singular vectors (SVs) are similar to adjoint sensitivity in that they also utilize the tangent linear propagator matrix  $M_{t,t_0}$ . Gelaro et al. (1999) provide an overview of how SVs can be obtained by calculating the eigenvectors of the eigenvalue/eigenvector problem:

$$(M_{t,t_0}^T * M_{t,t_0}) * u_i = \sigma_i^2 * u_i \tag{23.2}$$

where  $u_i$  are the orthogonal initial-time SVs of  $M_{t,t_0}$  (or eigenvectors of  $M_{t,t_0}^T * M_{t,t_0}$ ) with growth rates  $\sigma_i$ . The SVs with largest growth rates are the fastest growing perturbations with respect to the Euclidean norm  $(u_i^T * u_i)^{1/2}$ . Gelaro et al. (1999) show how the fastest growing perturbations with respect to more sophisticated norms, such as the dry total energy norm can be found, which adds additional weighting terms to equation (2) and presents a new eigenvalue/eigenvector problem that must be solved. In any case, the leading SVs reveal where errors would grow most rapidly with regard to a specified norm, and like adjoint sensitivity reveal areas where analysis error is undesirable with regard to the predictability of a specified aspect of the forecast state. For both adjoint sensitivity and SV applications, perturbation growth is measured about a previously run forecast. Both methods possess errors associated with the assumption of linear perturbation growth and the lack of a tangent-linear propagator containing the linearization of certain complex physics that exist in the full nonlinear model.

Perhaps motivated by studies that supported the notion of key analysis errors in regions of large adjoint sensitivity and leading SVs being most detrimental to forecasts (Rabier et al. 1996; Klinker et al. 1998), early observation targeting techniques were based on these locations. The basic idea was that by reducing errors where they would grow rapidly is the most effective way to improve forecasts. Buizza and Montani (1999), Gelaro et al. (1999), Langland et al. (1999), and Liu and Zou (2001) all found that by ingesting targeted observations in areas of leading SVs or large adjoint sensitivity, significant forecast error reductions (from 10 % to 50 %) were produced. These studies revealed the usefulness and value of SV and

sensitivity-based targeting for improving forecasts, and similar methods are still in use today with regard to high-impact weather events such as tropical cyclones (Reynolds et al. 2009).

Early efforts were also made to account for analysis uncertainty in addition to dynamical error growth through SV or adjoint sensitivity techniques. Taking into account analysis uncertainty is important because if observations are taken and assimilated in regions based on leading SVs, for example, they would have little impact if the background uncertainty was very small because the data assimilation system would essentially ignore the targeted observations. In turn, other locations with less-amplifying SVs may produce larger forecast impacts if large uncertainty and larger analysis increments were produced there, even if the dynamical error growth rates of those perturbations were smaller. Barkmeijer et al. (1998) addressed this issue with Hessian SVs, which are calculated with a norm based on analysis uncertainty provided by a 3DVAR system at initial time. Bishop and Toth (1999) developed the ensemble transform method, which accounts for uncertainty within the framework of an ensemble.

A major step forward in observation targeting techniques came with the realization that the characteristics of the data assimilation system used to assimilate the targeted observations should be considered. Data assimilation systems not only provide background uncertainty estimates at initial time, but also include observation error estimates, and contain the exact procedure that would be used to assimilate targeted observations. In turn, by considering both the assimilation characteristics and a way to estimate error growth (such as through SVs or adjoint sensitivity), more appropriate observation targeting techniques can be formulated that estimate more accurately how hypothetical observations would impact forecasts in a specific assimilation system. Both Berliner et al. (1999) and Langland (2005) elaborate on the necessity to include error evolution dynamics, analysis uncertainty, observation errors, and the specific assimilation system in formulating observation targeting schemes. This holistic approach to targeted observing laid the groundwork for modern adaptive data assimilation techniques using variational and ensemble methods.

Modern adaptive data assimilation was marked by the extension of initial condition sensitivity into observation sensitivity, and was first described in Baker and Daley (2000) in the context of a 3DVAR system. Observation sensitivity describes not how perturbations to initial conditions would change the forecast (as adjoint sensitivity does), but how an assimilated observation would change the forecast, and can be written as:

$$\partial R / \partial \mathbf{y}_o = \partial R / \partial \mathbf{x}_o * \partial \mathbf{x}_o / \partial \mathbf{y}_o \quad (23.3)$$

where  $\partial R / \partial \mathbf{y}_o$  is the observation sensitivity, which is a function of the adjoint sensitivity and the change to the analysis given observations ( $\partial \mathbf{x}_o / \partial \mathbf{y}_o$ ). For data assimilation systems that assume Gaussian statistics to achieve a most-likely state, the term  $\partial \mathbf{x}_o / \partial \mathbf{y}_o$  simply becomes the Kalman gain matrix. Equation (23.3) is a form of observation targeting as described in Baker and Daley (2000) as it allows one to

estimate the impact on a response function  $R$  due to innovations ( $\Delta\mathbf{y}_o$ ) with the calculation:

$$\Delta R = \partial R / \partial \mathbf{y}_o * \Delta \mathbf{y}_o \quad (23.4)$$

The only drawback of this method is that innovations associated with hypothetical observations are not known prior to obtaining the observations, although the technique is still very useful for understanding relative forecast impacts from a fixed innovation anywhere in the model domain.

Langland and Baker (2004) derived the observation impact methodology directly from (23.3) and (23.4), noting that  $\Delta R$  is composed of a sum of terms, each term containing a coefficient representing a different innovation (and thus a different observation). In this way, the contribution from each observation or any subset of observations to  $\Delta R$  can be easily calculated, and the impact of different, assimilated observations or subsets of observations can easily be produced. Conceptually, this is equivalent to the analysis increment produced from a specific set of assimilated observations projected onto the adjoint sensitivity field, yielding an estimate of  $\Delta R$ . This technique is the foundation for a number of observation impact studies (Langland and Baker 2004; Tremolet 2008; Gelaro and Zhu 2009; Gelaro et al. 2010), although these studies expand the observation impact method to account for nonlinear terms in the definition of the response function. Errico (2007) and Gelaro et al. (2007) discuss the accuracy of the expanded higher-order methodology, and also offer a more in depth interpretation of equation (3) noting that cross-correlations appear in each observational term that sum to produce  $\Delta R$ . The important issue these studies address through the observation impact technique is to understand which types of observations, such as those at different heights or those associated with different observational platforms, contribute to reducing forecast error and which do not. These results are crucial toward designing the most effective routine observational networks for operational assimilation/forecasting systems.

Significant observation impact and targeting developments were also made using ensemble data assimilation systems. Bishop et al. (2001) developed an ensemble transform Kalman filter (ETKF) observation targeting method based on the ensemble transform technique of Bishop and Toth (1999). The ETKF method is able to estimate the reduction in forecast variance due to hypothetical observations. A similar method was provided by Ancell and Hakim (2007a) within an EnKF assimilation system that also estimates the reduction in forecast variance of a chosen response function  $R$  due to hypothetical observations. This method is based on ensemble sensitivity which can be calculated in the following way (Ancell and Hakim 2007a):

$$\partial R / \partial \mathbf{y}_o = \text{Cov}(R, \mathbf{y}_o) * D^{-1} \quad (23.5)$$

where  $\partial R / \partial \mathbf{y}_o$  is a row vector representing the ensemble sensitivity of  $R$  with respect to each analysis variable,  $\text{Cov}(R, \mathbf{y}_o)$  is a row vector representing the covariance between the response function  $R$  and each analysis variable, and  $D$  is a diagonal matrix containing the variance of each analysis variable. Ancell and Hakim (2007a) explain that ensemble sensitivity allows one to estimate the perturbation to the response function  $R$  resulting from the temporal evolution of

an initial-time perturbation spread spatially and into other variables through the background error covariance relationships of the ensemble (similar to (23.4)). Since observational information is spread in a similar manner within the EnKF analysis procedure, and since the temporal evolution of perturbations can be represented with adjoint sensitivity, Ancell and Hakim (2007a) exploit the relationship between ensemble and adjoint sensitivity to derive an expression for the reduction in the variance of  $R$  due to a single observation within an EnKF:

$$\Delta \text{Variance}_R = (D_i * \partial R / \partial y_i)^2 / (D_i * O_i) \quad (23.6)$$

where  $D_i$  represents the variance of a single analysis variable,  $\partial R / \partial y_i$  is the ensemble sensitivity with respect to the same analysis variable, and  $O_i$  represents the observation error variance associated with a targeted observation. This calculation can be quickly made with respect to each observable analysis variable to reveal the estimated variance reduction from a single additional, hypothetical observation anywhere on the model domain. An advantage of these ensemble-based methods is that they rely not on actual observation values, but on observation error variance which exists prior to hypothetical observations being taken. They also allow the estimation of forecast variance reduction of additional targeted observations conditioned on the simultaneous assimilation of the initial targeted data. Ancell and Hakim (2007a) also derive an ensemble version of the observation impact developed in Langland and Baker (2004) without the use of an adjoint model. Liu and Kalnay (2008) discuss yet another ensemble-based observation impact technique that requires no adjoint model.

In summary, adaptive data assimilation techniques have evolved from those that consider only dynamical error growth to those that consider all aspects of the data assimilation system used to assimilate routine and targeted observations. In turn, modern adaptive data assimilation methods provide estimates of the impacts from assimilated or additional hypothetical observations with regard to a specific assimilation system such as 3DVAR or an EnKF. It should be noted that nearly all observation impact/targeting techniques are based on the assumption that error evolution is linear over the duration of the forecast, an assumption that doesn't always hold. Furthermore, both modern data assimilation systems and forecasting models are not perfect, and present another source of error for observation impact and targeting schemes. Langland (2005) provides an excellent review of the potential impacts these issues cause, and discusses the performance of different adaptive data assimilation methods during a variety of recent field programs. As computational resources are constantly improving, investigating adaptive assimilation techniques at very high resolution (grid spacing of a few kilometers) is now becoming possible. In turn, a major research focus in the coming years will likely be on the application of adaptive data assimilation systems at different scales.

### 23.3 Application of EnKF Observation Targeting to Land-Falling Mid-Latitude Cyclones

We now apply the EnKF observation targeting methodology of Ancell and Hakim (2007a) to understand the nature of the impacts of hypothetical observations beyond those of routine data for land-falling mid-latitude cyclones on the west coast of North America. Land-falling cyclones routinely produce heavy precipitation and high winds in coastal regions, and their predictability characteristics are thus important to understand. Mass and Dotson (2010) describe some of the most intense cyclones to strike the west coast of North America, and discuss the major societal impacts they produced. McMurdie and Mass (2004) and Wedam et al. (2009) describe how short-term forecast errors by deterministic operational numerical models can be large for storms impacting the west coast. The purpose of this study is to demonstrate how adaptive assimilation techniques can be applied retrospectively to cases of land-falling cyclones as a research tool to investigate the role of additional observations within a specific assimilation system and observing network.

#### 23.3.1 Details of the EnKF and the Forecast Model

The EnKF used in this study is an ensemble square-root filter that assimilates observations serially (Whitaker and Hamill 2002) and was created at the University of Washington (Torn and Hakim 2008). The 80-member EnKF runs on a 6-h update cycle on the modeling domain shown in Fig. 23.1 at 36-km grid spacing with 37 vertical levels. The routine observations that are assimilated are cloud-track wind (typically from 1,000 to 4,000 total), acars aircraft wind and temperature (typically from 1,000 to 4,000 total), radiosonde wind, temperature, and relative humidity (typically around 1,500 total), and surface wind, temperature, and altimeter data (typically from 7,000 to 10,000 total). The EnKF uses both Gaspari-Cohn horizontal localization (Gaspari and Cohn 1999) and posterior inflation to address sampling error and to avoid filter divergence (Anderson and Anderson 1999). The inflation and localization parameters used in this study are the same as those in Torn and Hakim (2008) which were tuned over a similar domain to produce appropriate spread and minimum ensemble mean errors. Boundary conditions were perturbed around the Global Forecasting System (GFS) analyses and forecasts using the fixed covariance perturbation method of Torn et al. (2006).

The EnKF was cycled for 6 months from 0000 UTC October 1, 2009 to 1800 UTC March 31, 2010, and extended ensemble forecasts were run to 24-h forecast time to capture a number of wintertime land-falling cyclones. The forecast model used here is the Advanced Research Weather Research and Forecasting (WRF-ARW) model Version 3.0.1.1 (Skamarock et al. 2008). The WRF physics used are the Mellor-Yamada-Janjic (MYJ) planetary boundary layer scheme (Janjic 1990, 1996, 2002), the Kain-Fritsch cumulus parameterization (Kain and Fritsch 1990,

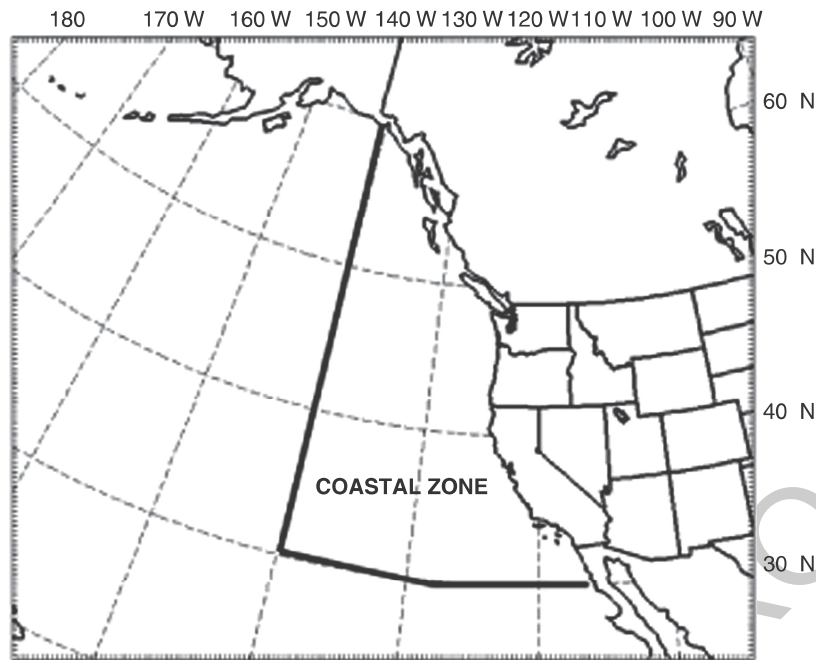


**Fig. 23.1** The EnKF domain used in this study. The coastal zone used to identify land-falling mid-latitude cyclones is outlined by the *thick black lines* and the North American coastline

1993), the Noah land surface model (Chen and Dudhia 2001), WRF Single-Moment 3-class microphysics (Hong et al. 2004), the Rapid Radiative Transfer Model (RRTM) longwave radiation scheme (Mlawer et al. 1997), and the Dudhia shortwave radiation scheme (Dudhia 1989).

### 23.3.2 *Description of the Response Function and Case Selection*

The response function used in these experiments to diagnose land-falling cyclones is the average sea-level pressure in a 216 km by 216 km box surrounding the 24-h forecast ensemble mean cyclone center. Only cyclones that could be identified as a local minimum and tracked back for the 24-h forecast period were included. Observation targeting calculations based on the methodology of Ancell and Hakim (2007a) are performed for every 24-h forecast cyclone that was found in the coastal zone (outlined in Fig. 23.1) over the 6-month duration of this study. A total of 27 storms were found to impact the coastal zone over this time, which is a typical frequency for wintertime land-falling cyclones. However, each storm lasted for several days and its position at the 24-h forecast time would be within the coastal zone over several consecutive forecast runs. Therefore, targeting calculations were made several times for each storm, resulting in a total of roughly 200 cases. Table 23.1 characterizes each forecast run of these storms with regard to their deepening rate and direction of coastal approach, two aspects that are analyzed later in this section. It should be noted that it was not possible to characterize each of the 27 individual storms as deepening or decaying as a particular event may

**Table 23.1** The total number of cyclones as well as those counted as deepening or decaying, or coming from the north, northwest, west, southwest, or south in this study

Cyclone characteristic	Number	
Deepening	37	t23.1
Decaying	87	t23.2
From the north	4	t23.3
From the northwest	19	t23.4
From the west	37	t23.5
From the southwest	48	t23.6
From the south	16	t23.7
All cyclones	198	t23.8

have forecast runs early in its lifetime when it deepens and forecast runs later in its lifetime when it decays. In the subsequent discussion, we will use ‘storms’ to refer to unique cyclones (i.e. the 27 storms) and ‘cyclones’ to refer to the individual forecast runs (i.e. one of the 200 samples).

The observation targeting calculations indicate the estimated variance reduction to the response function due to the assimilation of hypothetical temperature, wind, and pressure observations at analysis time *beyond* the assimilated routine data. In turn, the largest variance reduction values reveal the locations where an initial-time observation would reduce the uncertainty of the 24-h response function the most.

### 23.3.3 *Characteristics of Observation Targeting for a Single Cyclone*

Figure 23.2 shows the 00-h, 12-h, 18-h, and 24-h ensemble mean forecast initialized at 0600 UTC November 9, 2009 that depicts one particular cyclone that made landfall on the west coast of North America. This cyclone decays from 986-hPa central pressure in the analysis to 993-hPa central pressure when it makes landfall on the Canadian coast at 24-h forecast time. The targeting regions for winds, temperature, and pressure valid at analysis time are shown in Fig. 23.3, and are plotted at the level where the maximum value of estimated variance reduction was found. The targeting regions based on temperature and winds are localized and mesoscale in nature, which is generally the case for most land-falling cyclones during the 2009/2010 winter season (not shown). The targeting regions based on pressure are more typically characterized by synoptic-scale features, which is the case in Fig. 23.3. The largest targeting regions based on winds and pressure for this specific cyclone are found in the lower troposphere (from roughly 880 to 750 hPa for winds, 930 hPa for pressure), and near the tropopause (roughly 380 hPa) for temperature. Targeting regions based on all four observation types reveal areas in the immediate vicinity of the incipient system at analysis time, with wind and temperature targets aloft flanking the central position of the 500-hPa geopotential height minimum, and the primary pressure targets positioned just over the cyclone center at the surface. Dynamically, the primary zonal and meridional wind targets exist north and south (for zonal wind) and east and west (for meridional wind) of the cyclone center aloft, suggesting the effects of observations there would beneficially

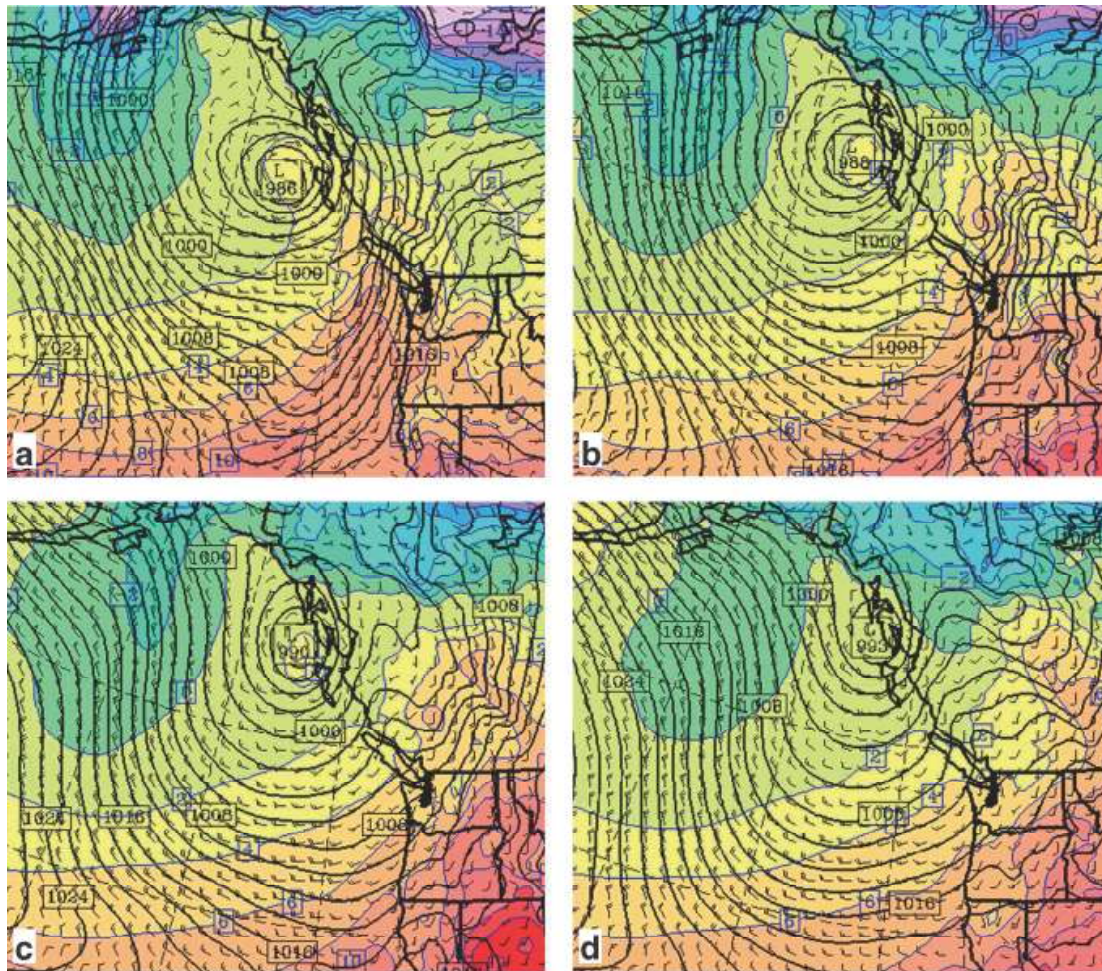


**Fig. 23.2** Ensemble mean forecast initialized at 0600 UTC November 9, 2009 of a decaying mid-latitude cyclone making landfall on the North American coastline valid at (a) 00-h, (b) 12-h, (c) 18-h, and (d) 24-h. Black contours represent sea-level pressure (contour interval is 2 hPa), blue contours represent 925-hPa temperature (contour interval is 2°C), and wind barbs represent 10-m winds

alter the cyclonic wind field flowing around the cyclone. Magnitudes of the variance 321  
reduction field are largest for pressure (reaching just over 1.4 hPa<sup>2</sup>), are slightly less 322  
for the wind field (reaching about 1.2 hPa<sup>2</sup>), and are smallest for the temperature 323  
field (reaching about 0.9 hPa<sup>2</sup>). 324

One interesting and unique feature of the targeting regions based on pressure in 325  
Fig. 23.3 is that they are less localized and show some impact away from the center 326  
of the system. Although values in these more distant regions are not as large as 327  
those in the immediate vicinity of the cyclone, they clearly highlight features in the 328  
flow at analysis time. Both the frontal trough near 40°N, -130°W and the large 329  
oceanic region of high pressure in the western portion of the domain are shown to 330  
be relatively important. In tune with the discussion of Ancell and Hakim (2007a), 331  
these features are highlighted as targets because they reveal areas where analysis 332  
increments would project substantially onto regions of large dynamical sensitivity 333  
(a quantity estimated through adjoint sensitivity analysis). This in turn reveals a 334  
defining characteristic of observation sensitivity over that of adjoint sensitivity— 335

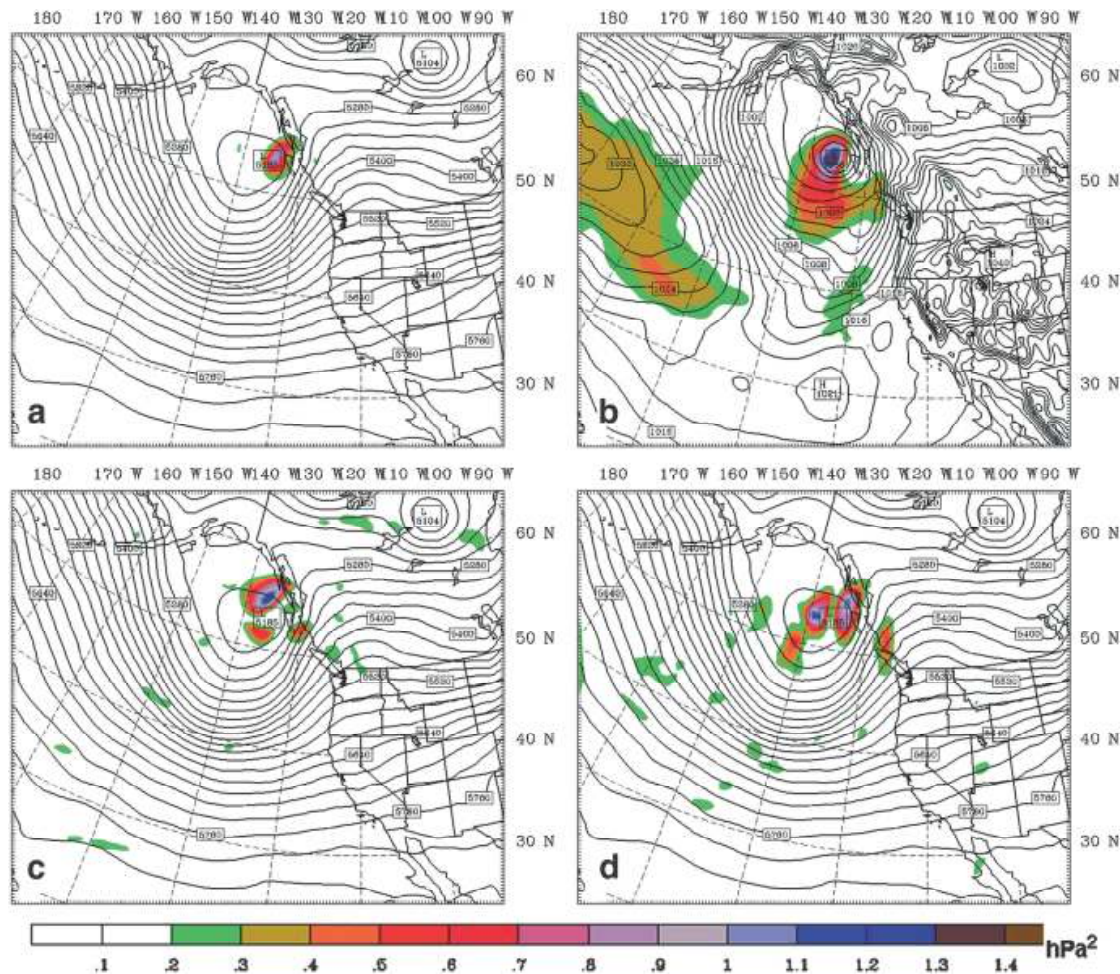


**Fig. 23.3** Variance reduction (*shaded*,  $\text{hPa}^2$ ) of the response function estimated from a single observation at the level of the maximum variance reduction for (a) temperature ( $\sim 380$  hPa), (b) pressure ( $\sim 930$  hPa), (c) zonal wind ( $\sim 750$  hPa), and (d) meridional wind ( $\sim 880$  hPa) valid at 0600 UTC November 9, 2009. Ensemble mean sea-level pressure (panel b, *black contours*, contour interval is 2 hPa) and 500-hPa geopotential height (panels a, c, and d, *black contours*, contour interval is 30 m) are also shown

observation targets can exist in relatively distant areas from the regions of large 336  
 adjoint sensitivity, sometimes indicating larger impacts than the regions of large 337  
 adjoint sensitivity itself. An important consequence of this characteristic are that 338  
 targeting regions based on observation sensitivity can differ strongly from those 339  
 based on adjoint sensitivity, indicating the importance of observation sensitivity 340  
 for adaptive data assimilation techniques as discussed in Sect. 23.2. As pointed 341  
 out, Fig. 23.3 shows the Pacific high surface pressure to be an important targeting 342  
 region, even though it is likely far upstream from the area of large adjoint sensitivity 343  
 (typical adjoint sensitivity fields associated with cyclones are shown by Ancell and 344  
 Mass 2006; Ancell and Hakim 2007a, b in similar experimental configurations). 345  
 Although perturbing this area of high pressure itself would do little to the 24-h 346  
 forecast of the land-falling cyclone, information spread during assimilation of 347  
 observations of the area of high pressure into regions of large dynamic sensitivity 348  
 downstream would act to significantly influence the forecast of the cyclone. 349

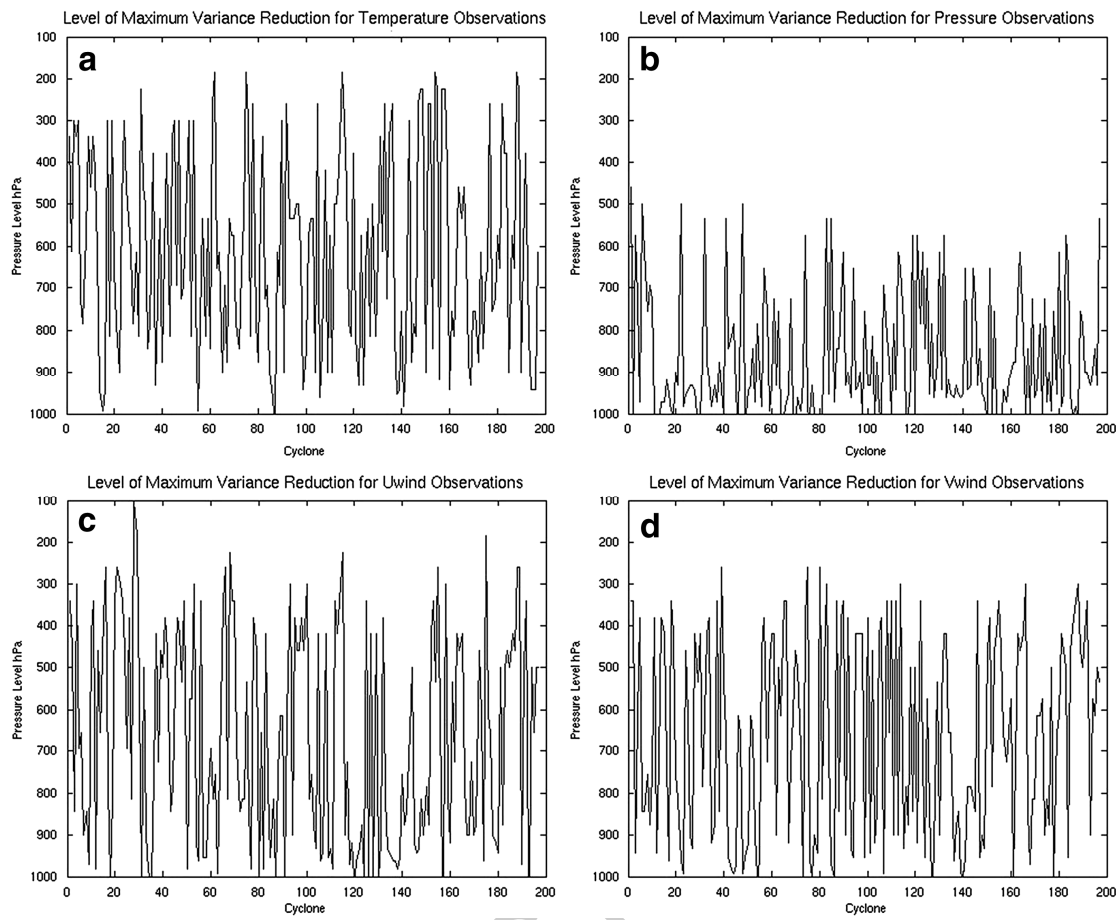
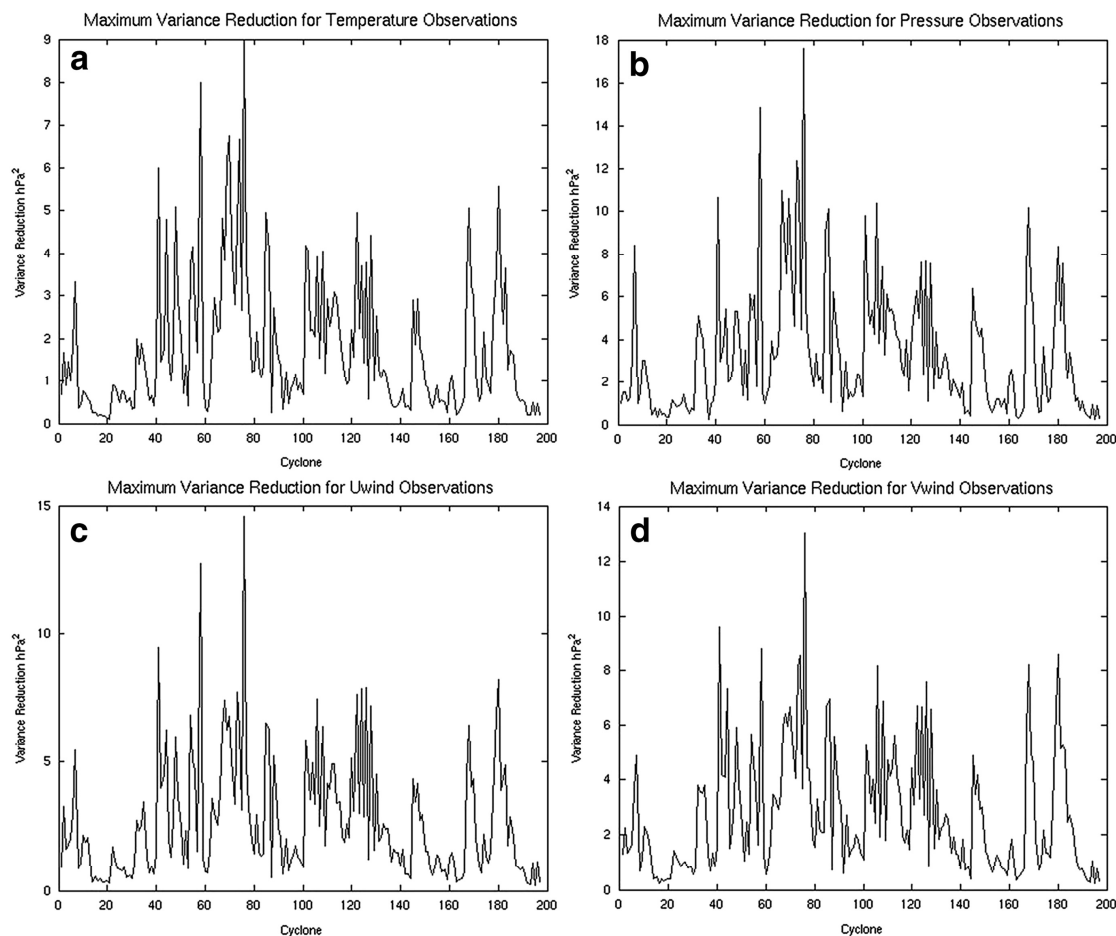


**Fig. 23.4** Level of maximum variance reduction of the response function for all cyclones for observations of (a) temperature, (b) pressure, (c) zonal wind, and (d) meridional wind

The fact that targeting regions are clearly co-located with features in the flow is likely a unique feature of ensemble targeting techniques. Following the discussion above, the impacts from hypothetical observations within an EnKF highlight specific flow features through their relationship to dynamically sensitive areas. In turn, these relationships depend on how the specific features in each ensemble member covary with the dynamically sensitive regions, and are thus strongly linked to the flow dependence present in the atmospheric state at any given time. Consequently, covariances that do not possess such flow dependence are unlikely to capture these relationships, and targeting regions based on 3DVAR systems will probably differ to some degree from those based on ensemble methods. This further stresses the importance of directly accounting for the specific assimilation system when calculating the impacts of targeted observations.

### 23.3.4 Characteristics of Observation Targeting for all 2009/2010 Cyclones

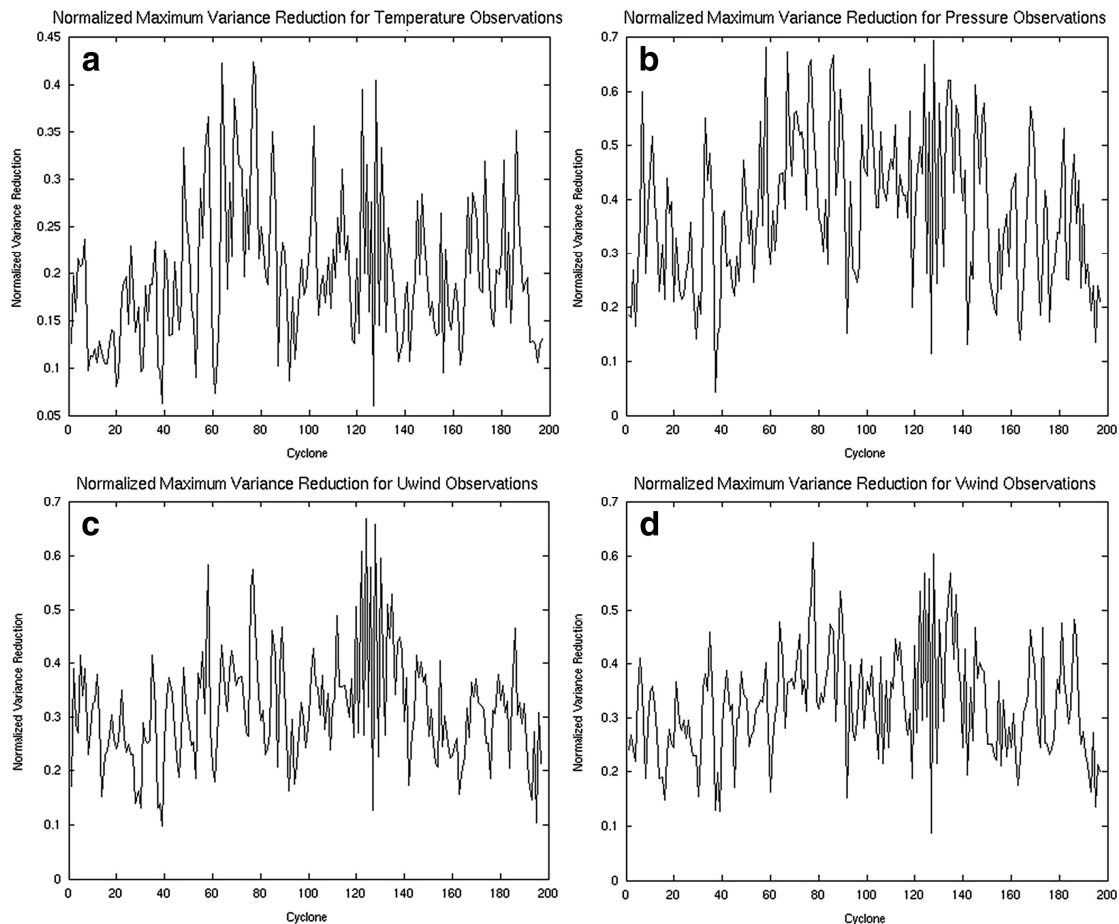
Figure 23.4 represents the level where the maximum variance reduction exists for each cyclone for pressure, temperature, and wind observations. For both temperature



**Fig. 23.5** Value of maximum variance reduction ( $\text{hPa}^2$ ) of the response function for all cyclones for observations of (a) temperature, (b) pressure, (c) zonal wind, and (d) meridional wind

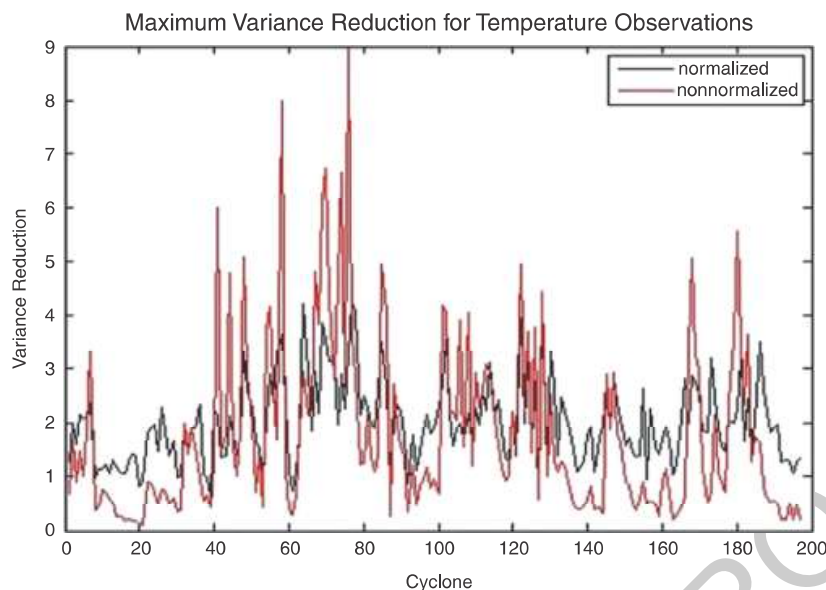
and wind, the level of maximum values exists throughout the troposphere, whereas 366  
 for pressure the maximum levels are confined to the lower half of the troposphere 367  
 below 500 hPa. Furthermore, the level of maximum variance reduction is near the 368  
 surface for pressure observations for a large number of cyclones. This suggests a 369  
 substantial benefit might be gained by assimilating scatterometer sea-level pressure 370  
 retrievals, such as those that used to be provided by the QuickSCAT satellite, with 371  
 regard to forecasts of North American land-falling mid-latitude cyclones. 372

Figure 23.5 depicts the maximum values of variance reduction for each cyclone, 373  
 regardless of vertical level, for each observation type. As shown in Fig. 23.3, the 374  
 largest values are associated with pressure observations. For all observations, 375  
 significant variability exists with these maximum values as they range from near 376  
 zero to about 15  $\text{hPa}^2$  for winds, to about 9  $\text{hPa}^2$  for temperature, and to roughly 377  
 18  $\text{hPa}^2$  for pressure. Interestingly, the maximum values for all observation types 378  
 follow the same general trend. When a cyclone exhibits large maximum variance 379  
 reduction for one type of observation (e.g. pressure), it also exhibits large maximum 380  
 variance reduction for the other types of observations (wind and temperature). This 381  
 property reveals that the largest impacts of targeted observations for the cyclones in 382  
 this study are independent of observation type. 383



**Fig. 23.6** Value of maximum variance reduction of the response function normalized by the response function variance for all cyclones for observations of (a) temperature, (b) pressure, (c) zonal wind, and (d) meridional wind

It is also useful to describe targeting impacts in terms of the estimated variance 384  
reduction relative to the response function variance. This can be done by dividing 385  
the maximum variance reduction values by the original response function 386  
resulting in what is referred to here as normalized variance reduction. In this 387  
way, it is possible to reveal cases where observations might reduce a substantial 388  
fraction of the original response function variance even if the actual variance 389  
reduction values themselves (as shown in Fig. 23.5) are quite small. Figure 23.6 390  
shows the normalized maximum values of estimated variance reduction, and reveals 391  
the percentage of response function variance that could be reduced through the 392  
assimilation of observations. In general, pressure observations show an estimated 393  
34 % variance reduction averaged over all cyclones, which is larger than both wind 394  
(23 %) and temperature (12 %). As with the absolute values in Fig. 23.5, the trend 395  
among all variables remains the same. Figure 23.7 depicts both the normalized and 396  
absolute maximum values of variance reduction with regard to temperature for all 397  
cyclones. The trend for both the normalized and absolute values is generally similar 398  
for all cyclones, although there are localized differences in the plots. For example, 399  
the peaks in the normalized and non-normalized values between cyclone number 30 400



**Fig. 23.7** Both normalized (nondimensional) and non-normalized ( $\text{hPa}^2$ ) values of maximum variance reduction of the response function for all cyclones for observations of temperature. Normalized values are multiplied by 10 for ease of comparison with non-normalized values

and 40 are offset. This indicates that whereas a larger absolute variance reduction is estimated from temperature observations at the peak of the non-normalized values, the response function variance must be somewhat larger for that cyclone such that the estimated fraction of response function variance is smaller. This indicates that for specific cases, the impacts of EnKF targeted observations can be viewed with differing degrees of importance depending on whether these impacts are determined by the total or the fraction of estimated response function variance reduction.

Another interesting result that can be found by analyzing targeted observations for many cases is how the location of the most significant targeting locations vary in time. For a specific high-impact weather event, if the targeting regions remained constant over many cases, strong support would exist for taking routine observations in those locations. If targeting regions were not constant, the degree to which they vary would provide crucial information toward how to best design an adaptive observing network. Figure 23.8 shows the mean estimated maximum variance reduction calculated over all cyclones throughout the vertical. Interestingly, pressure observations show roughly a constant impact throughout the troposphere. This reveals that although the maximum estimated targeting values tend to occur in the lower atmosphere for pressure observations (Fig. 23.4), values are nearly constant within the entire troposphere. In turn, there are no preferred targeting locations in the vertical with regard to pressure observations to improve land-falling cyclone forecasts. Wind and temperature observation targeting regions, however, show two distinct peaks in the vertical. Wind targeting regions show peaks near 400 hPa and the surface, whereas temperature targeting regions reveal the 250-hPa and the 600-hPa levels to be most important. It seems reasonable that the important temperature targeting locations near 250-hPa are due to large variance near the

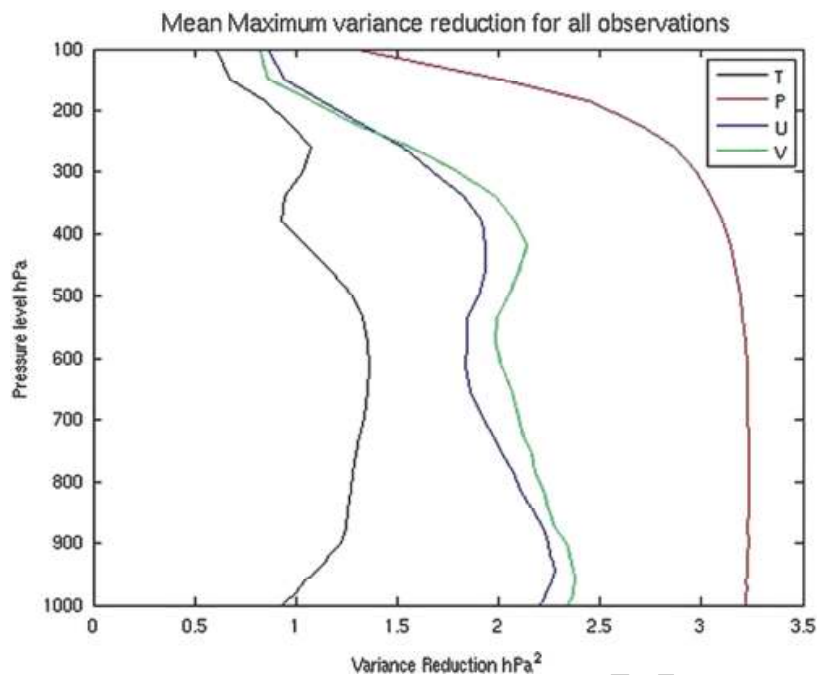


**Fig. 23.8** Value of maximum variance reduction of the response function averaged over all vertical model levels for all cyclones for all observation types

tropopause involved with the general temperature minimum at that level. It is not obvious why the 600-hPa level is important, or why wind targeting locations are important near the surface and at 400 hPa. Either large ensemble-based sensitivity or analysis variance values would contribute to large estimated variance reduction values, and it is thus likely one of these two quantities is consistently larger at the levels where the peaks are evident in Fig.23.8. In any case, these levels indicated preferred locations where on average, supplemental temperature and wind observations would be most beneficial.

Figure 23.9 shows the horizontal locations of the maximum estimated variance reduction for temperature observations organized by cyclones that approach the coastal zone from the northwest, west, southwest, and south. Cyclones along these tracks have been binned over a 45° swath centered on each direction listed. The locations are shown relative to the 24-h forecast position of the ensemble mean cyclone. It is clear that for all cyclone tracks there is significant variability in the horizontal location of the maximum variance reduction values, varying up to about 40° both longitudinally and latitudinally. Interestingly, a number of the maximum variance reduction locations occur at or downstream of the 24-h forecast position of the cyclone, indicating the ability of the EnKF to spread observational information upstream into regions where large dynamical sensitivity is likely to exist. Nonetheless, it seems the highest priority targeting regions rarely exist in the same location relative to the forecast position of the cyclone. Although there is some clustering of maximum variance values to the southwest of cyclones that approach from the southwest, there is still a large spread in the location of maximum variance reduction such that the chance that a single location would provide consistently large

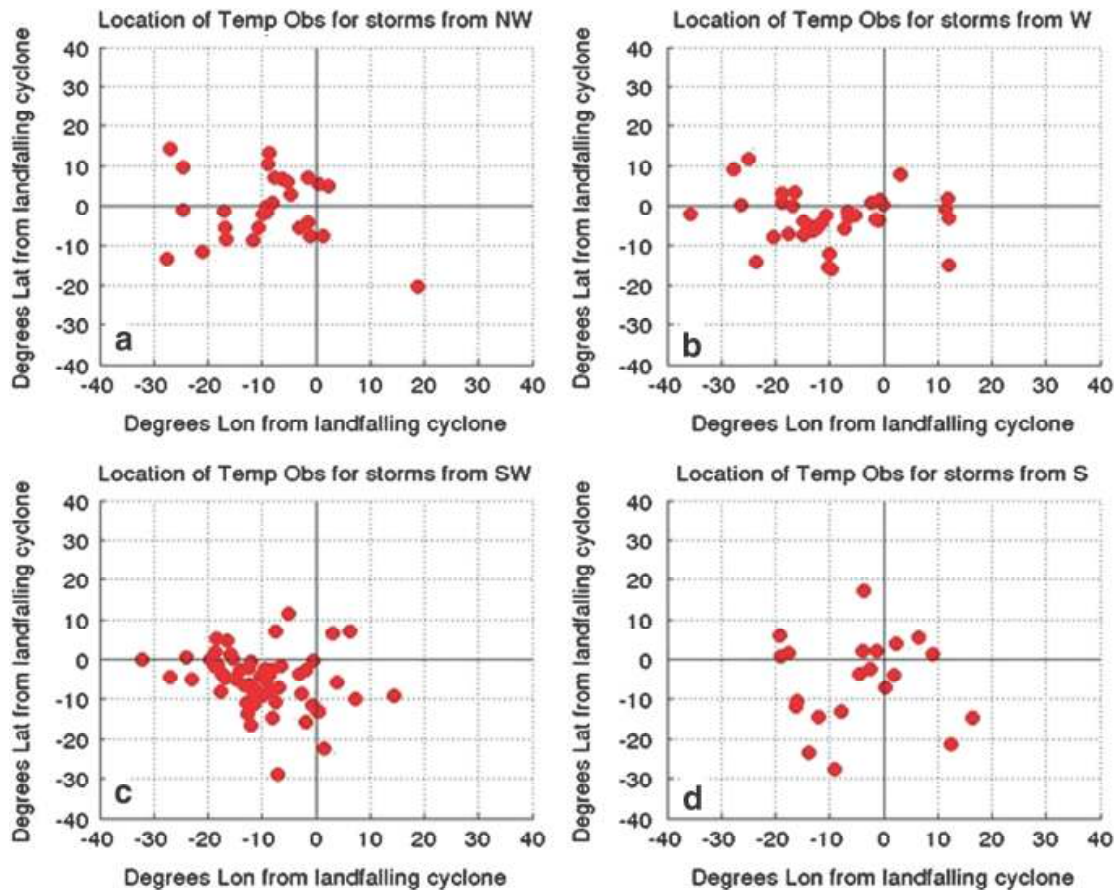


Fig. 23.9 Horizontal location relative to the 24-h forecast cyclone position of the maximum variance reduction of the response function for temperature observations for cyclones approaching the coastal zone from the (a) northwest, (b) west, (c) southwest, and (d) south

positive forecast benefits is unlikely. This is especially true since these locations are 450  
 relative to the forecast position of the cyclone, and less clustering would be evident 451  
 when considering the actual positions of the maximum variance reduction values 452  
 within the modeling domain. Very similar results are found regarding the horizontal 453  
 location of targeting sites for pressure and wind observations (not shown). 454

Figure 23.10 depicts the average maximum variance reduction for all observation 455  
 types segregated by whether the cyclone was deepening or decaying over the 24-h 456  
 forecast period. The error bars represent the 95 % confidence interval. For each 457  
 observation type, deepening cyclones are associated with larger variance reduction 458  
 values on average, implying that observation targeting is more effective for deepening 459  
 cyclones. This result is not reproduced when considering cyclone track, as the 460  
 average variance reduction values in Fig. 23.11 are essentially indistinguishable at 461  
 the 95 % confidence level among different cyclone tracks. These results demonstrate 462  
 how targeting impacts can relate to certain characteristics of the high impact event 463  
 in question (in this case the deepening rate of land-falling cyclones). 464

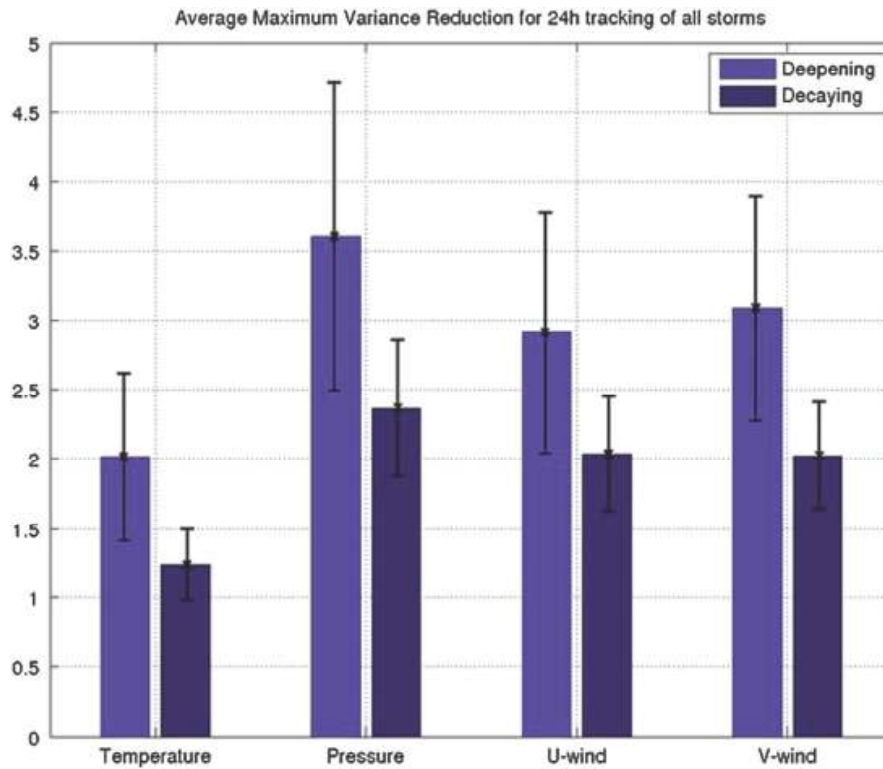


Fig. 23.10 Average value of the maximum variance reduction of the response function for all observation types for both deepening (light purple) and decaying (dark purple) cyclones

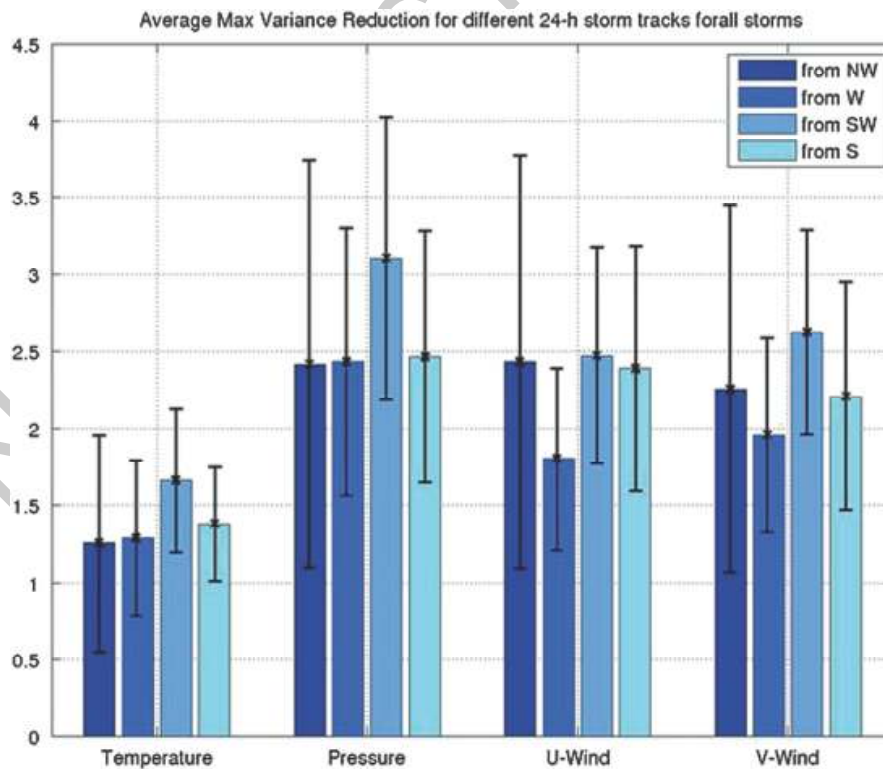


Fig. 23.11 Average value of the maximum variance reduction of the response function for all observation types for cyclones approaching the North American coast from the northwest, west, southwest, and south

### 23.3.5 Summary and Concluding Remarks

465

Observation targets of pressure, winds, and temperature within an EnKF for land-falling Pacific cyclones on the west coast of North America were examined for a 6-month wintertime synoptic period in 2009/2010. These targets represented estimates of where assimilated hypothetical observations beyond assimilated routine observations would produce the largest reduction in the uncertainty of 24-h cyclone forecasts around the time of landfall. It was found that temperature and wind targets were mesoscale in nature, whereas pressure targets were more prominent on the synoptic scale. Furthermore, pressure observations produced the largest positive impacts on the uncertainty of cyclone forecasts of the four observation types examined. The most important targeting regions in the vertical for winds and temperature varied substantially throughout the troposphere when considering all cyclones, but there was an indication of preferred regions in the mid- and upper-troposphere for temperature and the upper-troposphere and near the surface for winds. Although the largest benefits from pressure observations existed near the surface, similar benefits existed throughout the troposphere with no clear preferred level. In the horizontal, there was significant variability in the most important targeting areas, showing no clear location where a routine observation would be consistently beneficial to land-falling cyclone forecasts. Lastly, it was found that targeted observations are more beneficial to forecasts of deepening cyclones than to decaying systems as they approach the coast. This result was not found when considering the directions along which the cyclones track as cyclones from all directions showed similar benefits from targeted observations.

It is important to note that the best way to view the results presented here is in a relative sense. Specifically, these experiments have provided an understanding of how impacts vary within an EnKF among the different observation types of pressure, winds, and temperature for land-falling mid-latitude cyclones. Whether these results extend to other assimilation systems and different high-impact events is unclear. Furthermore, the estimated variance reductions in this study are based on ensemble sensitivity, and thus the particular variance reduction values would need to be compared with experiments that actually assimilate targeted observations to understand the relationship between estimated and actual forecast impacts. The effects of nonlinearity, inflation, and localization may all play a role in any discrepancy. Nonetheless, this study has provided a unique perspective on how targeting techniques might be designed to best benefit forecasts of land-falling Pacific cyclones. Lastly, as assimilation and forecasting systems at higher and higher resolution become more feasible in the coming years, gaining an understanding of the effects of targeted observations across multiple scales will be an intriguing endeavor.

## References

504

- Ancell BC, Hakim GJ (2007a) Comparing adjoint and ensemble sensitivity analysis with applications to observation targeting. *Mon Weather Rev* 135:4117–4134 505
- Ancell BC, Hakim GJ (2007b) Interpreting adjoint and ensemble sensitivity toward the development of optimal observation targeting strategies. *Met Zeitschrift* 16:635–642 507
- Ancell BC, Mass CF (2006) Structure, growth rates, and tangent linear accuracy of adjoint sensitivities with respect to horizontal and vertical resolution. *Mon Weather Rev* 134:2971–2988 509
- Anderson JL, Anderson SL (1999) A Monte Carlo implementation of the nonlinear filtering problem to produce ensemble assimilations and forecasts. *Mon Weather Rev* 127:2741–2758 511
- Baker N, Daley R (2000) Observation and background sensitivity in the adaptive observation-targeting problem. *Q J Roy Meteorol Soc* 126:1431–1454 513
- Barkmeijer J, Bouttier F, Gijzen MV (1998) Singular vectors and estimates of the analysis-error covariance metric. *Q J Roy. Meteorol. Soc* 124:1695–1713 514
- Berliner ML, Lu Z-Q, Snyder C (1999) Statistical design for adaptive weather observations. *J Atmos Sci* 56:2536–2552 516
- Bishop CH, Toth Z (1999) Ensemble transformation and adaptive observations. *J Atmos Sci* 56:1748–1765 518
- Bishop CH, Etherton BJ, Majumdar SJ (2001) Adaptive sampling with the ensemble transform Kalman filter. Part I: theoretical aspects. *Mon Weather Rev* 129:420–436 521
- Buizza R, Montani A (1999) Targeting observations using singular vectors. *J Atmos Sci* 56:2965–2985 522
- Chen F, Dudhia J (2001) Coupling an advanced land-surface/hydrology model with the Penn State/NCAR MM5 modeling system. Part I: model description and implementation. *Mon Weather Rev* 129:569–585 524
- Dudhia J (1989) Numerical study of convection observed during the winter monsoon experiment using a mesoscale two-dimensional model. *J Atmos Sci* 46:3077–3107 526
- Errico RM (1997) What is an adjoint model? *Bull Am Meteorol Soc* 78:2577–2591 527
- Errico RM (2007) Interpretations of an adjoint-derived observational impact measure. *Tellus* 59A:273–276 528
- Gaspari G, Cohn SE (1999) Construction of correlation functions in two and three dimensions. *Q J Roy Meteorol Soc* 125:723–757 529
- Gelaro R, Zhu Y (2009) Examination of observation impacts derived from observing system experiments (OSEs) and adjoint models. *Tellus* 61A:179–193 530
- Gelaro R, Langland RH, Rohaly GD, Rosmond TE (1999) An assessment of the singular-vector approach to targeted observing using the FASTEX dataset. *Q J Roy Meteorol Soc* 125:3299–3327 531
- Gelaro R, Zhu Y, Errico RM (2007) Examination of various-order adjoint-based approximations of observation impact. *Met Zeitschrift* 16:685–692 532
- Gelaro R, Langland RH, Pellerin S, Todling R (2010) The THORPEX observation impact intercomparison experiment. *Mon Weather Rev* 138:4009–4025 533
- Hong S-Y, Dudhia J, Chen S-H (2004) A revised approach to ice microphysical processes for the bulk parameterization of clouds and precipitation. *Mon Weather Rev* 132:103–120 534
- Janjic ZI (1990) The step-mountain coordinate: physical package. *Mon Weather Rev* 118:1429–1443 535
- Janjic ZI (1996) The surface layer in the NCEP Eta Model. In: Proceedings of the eleventh conference on numerical weather prediction, American Meteorological Society, Norfolk, 19–23 Aug 1996, pp 354–355 536
- Janjic ZI (2002) Nonsingular implementation of the Mellor-Yamada Level 2.5 scheme in the NCEP Meso model. NCEP Office Note, No. 437, 61 p 537
- Kain JS, Fritsch JM (1990) A one-dimensional entraining/detraining plume model and its application in convective parameterization. *J Atmos Sci* 47:2784–2802 538

Kain JS, Fritsch JM (1993) Convective parameterization for mesoscale models: the Kain-Fritsch scheme. In: Emanuel KA, Raymond DJ (eds) <i>The Representation of Cumulus Convection in Numerical Models</i> , American Meteorological Society, Boston, 246 p	556 557 558
Kalnay E (2002) <i>Atmospheric modeling, data assimilation, and predictability</i> . Cambridge University Press, Cambridge, 364 p	559 560
Klinker E, Rabier F, Gelaro R (1998) Estimation of key analysis errors using the adjoint technique. <i>Q J Roy Meteorol Soc</i> 124:1909–1933	561 562
Langland RH (2005) Issues in targeted observing. <i>Q J Roy Meteorol Soc</i> 131:3409–3425	563
Langland RH, Baker NL (2004) Estimation of observation impact using the NRL atmospheric variational data assimilation adjoint system. <i>Tellus</i> 56A:189–201	564 565
Langland RH, Toth Z, Gelaro R, Szunyogh I, Shapiro MA, Majumdar SJ, Morss RE, Rohaly GD, Velden C, Bond N, Bishop CH (1999) The North Pacific Experiment (NORPEX-98): targeted observations for improved North American weather forecasts. <i>Bull Am Meteorol Soc</i> 180:1363–1384	566 567 568 569
LeDimet F, Talagrand O (1986) Variational algorithms for analysis and assimilation of meteorological observations: theoretical aspects. <i>Tellus</i> 38A:97–110	570 571
Liu J, Kalnay E (2008) Estimating observation impact without adjoint model in an ensemble Kalman filter. <i>Q J Roy Meteorol Soc</i> 134:1327–1335	572 573
Liu H, Zou X (2001) The impact of NORPEX targeted dropsondes on the analysis and 2–3-day forecasts of a landfalling Pacific winter storm using NCEP 3DVAR and 4DVAR systems. <i>Mon Weather Rev</i> 129:1987–2004	574 575 576
Mass CF, Dotson B (2010) Major extratropical cyclones of the northwest United States: historical review, climatology, and synoptic environment. <i>Mon Weather Rev</i> 138:2499–2527	577 578
McMurdie LA, Mass CF (2004) Major numerical forecast failures over the northeast Pacific. <i>Weather Forecast</i> 19:338–356	579 580
Mlawer EJ, Taubman SJ, Brown PD, Iacono MJ, Clough SA (1997) Radiative transfer for inhomogeneous atmosphere: RRTM, a validated correlated-k model for the longwave. <i>J Geophys Res</i> 102:16663–16682	581 582 583
Rabier F, Klinker E, Courtier P, Hollingsworth A (1996) Sensitivity of forecast errors to initial conditions. <i>Q J Roy Meteorol Soc</i> 122:121–150	584 585
Reynolds CA, Doyle JD, Hodur RM, Jin H (2009) Naval Research Laboratory Multiscale Targeting Guidance for T-PARC and TCS-08. <i>Weather Forecast</i> 25:526–543	586 587
Skamarock WC, Klemp JB, Dudhia J, Gill DO, Barker DM, Duda M, Huang X-Y, Wang W, Powers JG (2008) A description of the advanced research WRF version 3. NCAR Technical Note TN-475	588 589 590
Torn RD, Hakim GJ (2008) Performance characteristics of a pseudo-operational ensemble Kalman filter. <i>Mon Weather Rev</i> 136:3947–3963	591 592
Torn RD, Hakim GJ, Snyder C (2006) Boundary conditions for limited-area ensemble Kalman filters. <i>Mon Weather Rev</i> 134:2490–2502	593 594
Tremolet Y (2008) Computation of observation sensitivity and observation impact in incremental variational data assimilation. <i>Tellus</i> 60A:964–978	595 596
Wedam GB, McMurdie LA, Mass CF (2009) Comparison of model forecast skill of sea-level pressure along the east and west coasts of the United States. <i>Weather Forecast</i> 24:843–854	597 598
Whitaker JS, Hamill TM (2002) Ensemble data assimilation without perturbed observations. <i>Mon Weather Rev</i> 130:1913–1924	599 600 601

AQ3  
AQ4

AUTHOR QUERIES

- AQ1. Please check the corresponding author identity
- AQ2. Please provide details of "Kalnay (2003), Skamarock (2008)" in the reference list.
- AQ3. Please check if inserted publisher location for Kain and Fritsch (1993), Kalnay (2002) is okay.
- AQ4. Please cite "Kalnay (2002), Skamarock et al. (2008)" in text.

UNCORRECTED PROOF